HHS Public Access

Author manuscript

Neuroimage. Author manuscript; available in PMC 2018 March 22.

Published in final edited form as:

Neuroimage. 2018 March ; 168: 403–411. doi:10.1016/j.neuroimage.2016.09.023.

Individualized parcellation of the subthalamic nucleus in patients with Parkinson's disease with 7T MRI

Birgit R. Plantinga[a,b], **Yasin Temel**[a,c,*], **Yuval Duchin**[d], **Kâmil Uludağ**[e], **Rémi Patriat**[d], **Alard Roebroeck**[e], **Mark Kuijf**[f], **Ali Jahanshahi**[c], **Bart ter Haar Romenij**[b,g], **Jerrold Vitek**[h], and **Noam Harel**[d,**]

[a]Departments of Neuroscience, Maastricht University, Maastricht, Netherlands [b]Department of Biomedical Image Analysis, Eindhoven University of Technology, Eindhoven, Netherlands [c]Department of Neurosurgery, Maastricht University Medical Center, Maastricht, Netherlands [d]Center for Magnetic Resonance Research, University of Minnesota Medical School, Minneapolis, MN, USA [e]Department of Cognitive Neuroscience, Maastricht University, Maastricht, Netherlands [f]Department of Neurology, Maastricht University Medical Center, Maastricht, Netherlands [g]Northeastern University, Shenyang, China [h]Department of Neurology, University of Minnesota, Minneapolis, MN, USA

Abstract

Deep brain stimulation of the subthalamic nucleus (STN) is a widely performed surgical treatment for patients with Parkinson's disease. The goal of the surgery is to place an electrode centered in the motor region of the STN while lowering the effects of electrical stimulation on the non-motor regions. However, distinguishing the motor region from the neighboring associative and limbic areas in individual patients using imaging modalities was until recently difficult to obtain *in vivo*. Here, using ultra-high field MR imaging, we have performed a dissection of the subdivisions of the STN of individual Parkinson's disease patients.

We have acquired 7 T diffusion-weighted images of seventeen patients with Parkinson's disease scheduled for deep brain stimulation surgery. Using a structural connectivity-based parcellation protocol, the STN's connections to the motor, limbic, and associative cortical areas were used to map the individual subdivisions of the nucleus.

A reproducible patient-specific parcellation of the STN into a posterolateral motor and gradually overlapping central associative area was found in all STNs, taking up on average 55.3% and 55.6% of the total nucleus volume. The limbic area was found in the anteromedial part of the nucleus.

Our results suggest that 7T MR imaging may facilitate individualized and highly specific planning of deep brain stimulation surgery of the STN.

*Corresponding author at: Department of Neurosurgery, Maastricht University Medical Center, P. Debyelaan 25, 6202 AZ Maastricht, Netherlands, y.temel@maastrichtuniversity.nl. **Correspondence to: Center for Magnetic Resonance Research/Department of Radiology, University of Minnesota Medical School, 2021 6th Street SE, Minneapolis, MN 55455, USA. harel002@umn.edu.

Keywords

Subthalamic nucleus; Ultra-high field MRI; Deep brain stimulation; Parkinson's disease; Parcellation; Patient-specific

1. Introduction

Deep brain stimulation (DBS) of the subthalamic nucleus (STN) is a widely performed surgical treatment for patients with Parkinson's disease (PD) (Deuschl et al., 2006; Schuepbach et al., 2013). There are two determining factors for a successful outcome: patient selection (Okun et al., 2005) and accuracy of targeting (Okun et al., 2005; Paek et al., 2013; Welter et al., 2014). Concerning the latter, the STN is organized into three main functional territories: motor, associative and limbic regions and the goal of DBS is to preferentially stimulate the motor part of the STN to obtain optimal motor outcome. Targeting is currently performed with 1.5T or 3T MRI, usually combined with intra-operative micro-electrode recordings and patient testing to distinguish the motor part from the neighboring associative and limbic areas (Zaidel et al., 2010). In this context, behavioral side-effects have often been linked to undesired stimulation of the non-motor territories of the STN (Mallet et al., 2007; Okun et al., 2009).

Although the debate is still ongoing (Alkemade and Forstmann, 2014; Keuken et al., 2012; Lambert et al., 2015), classical neuroanatomical studies in animal models, place the motor territory in the posterolateral portion of the STN and the associative and limbic regions more anteromedially (Parent and Hazrati, 1995; Temel et al., 2005). Using a 3T clinical MR scanner, this anatomical concept was demonstrated in healthy subjects (Lambert et al., 2012). Compared to 3T MRI, ultra-high field (7T and higher) MRI technology promises to improve the imaging contrast, resolution, and signal-to-noise ratio at clinically feasible scan times (Abosch et al., 2010; Cho et al., 2010; Lenglet et al., 2012; Plantinga et al., 2014), which allows for a detailed visualization of the patients' STN anatomy and its connections (Abosch et al., 2010; Lenglet et al., 2012). In this study, we have acquired 7 T diffusion-weighted images of patients with PD scheduled for deep brain stimulation surgery. Using a previously established protocol applied on thalamic parcellation (Behrens et al., 2003), we have performed a patient-specific dissection of the subdivisions of the STN demonstrating a clear topographical organization of major functional territories that may allow for individualized surgical planning.

2. Materials and methods

2.1. Subjects

We have included seventeen patients with idiopathic PD (five female, ages: 48–74 years, mean age: 62 years, mean UPDRS-III on/off medication: 18.3/37.5) who were referred for DBS surgery at the University of Minnesota (Minneapolis, MN, USA) and Maastricht University Medical Center (Maastricht, Netherlands). The inclusion criteria for surgery were clinical findings consistent with idiopathic PD, severe response fluctuations and/or dyskinesias (despite optimal pharmacological treatment) and good initial L-dopa response.

The exclusion criteria were significant atrophy, focal brain abnormalities on MRI, a score of less than 24 on the Mini-Mental State Examination, psychosis, and general contraindications for surgery such as severe hypertension or blood coagulation disorders.

Subjects with claustrophobia or other contra-indications for 7T MRI (such as pacemakers and metallic implants) were also excluded from the study. This study was approved by the Institutional Review Board at the University of Minnesota and the Local Medical Ethics Committee at Maastricht University Medical Center.

2.2. Scanning protocol

Patients were scanned on a 7T MRI scanner (Magnetom 7T Siemens, Erlangen, Germany), available at both institutions, equipped with SC72 gradients capable of 70 mT/m and a 200 T/m/s slew rate using a 32-element head array coil (Nova Medical, Inc, Burlington, MA, USA), while taking their usual antiparkinsonian medication. Dielectric pads (Teeuwisse et al., 2012) were applied, when possible (n=11), to enhance signal in the temporal regions. The scan protocol consisted of a) a T1-weighted whole brain scan with an inversion time of 1500 ms, b) a T2-weighted coronal slab through the STNs, and c) a whole brain diffusion-weighted scan along 50 directions with a b-value of 1500 s/mm^2 and four additional b0-volumes, performed twice with anterior-posterior and posterior-anterior phase encoding directions. Details of the scan protocol can be found in Table 1. Five patients were scanned with a slightly different protocol, including a diffusion-weighted scan with a b-value of 2000 s/mm^2, 60 directions, and twelve b0-volumes of which six with opposite phase encoding directions, and a T2*-weighted 0.5 mm isotropic GRE-scan. These small protocol differences did not significantly alter the individual findings.

2.3. Image analysis

2.3.1. Cortical masks—A 1 mm^3 isotropic T1-weighted reference brain, developed by the Montreal Neurological Institute (MNI) (Grabner et al., 2006), was manually divided into four cortical areas: the motor, associative, and limbic cortical areas, and the remaining cortex (see Fig. 1). The motor area included the primary motor, supplementary motor, and pre-motor cortex. On the MNI brain, this was defined as the cortical area bounded posteriorly by the central sulcus, medially by the cingulate sulcus, laterally by the border between the precentral gyrus and frontal operculum gyrus, and anteriorly as defined by the human motor area template (Mayka et al., 2006). The limbic area was made symmetrical across hemispheres and included the orbitofrontal and entorhinal cortices based on the definition by Mai et al. (2008), and the anterior cingulate cortex, amygdala, and hippocampus as adopted from the Harvard-Oxford atlas (Desikan et al., 2006). The associative area was defined as the cortical region bounded by the limbic cortical area anteriorly and the motor cortical area posteriorly. The fourth cortical area consisted of the remaining cortex, including the occipital lobe, parietal lobe, and part of the temporal lobe. The MNI brain and cortical masks were non-linearly registered to each patient's T1-image with FSL's FNIRT (Andersson et al., 2007) and masked with gray matter segmentations of the T1-images produced with FSL's FAST (Zhang et al., 2001) that were dilated with one voxel. This resulted in four gray matter cortical masks in each subject's native space.

2.3.2. STN segmentations—For each subject, the STNs, which were visible as a hypointense structure superior to the substantia nigra in the coronal plane (Fig. 1), were manually segmented on the T2-weighted images with Amira software (FEI, Hillsboro, OR, USA). The good intra-observer agreement index for segmentations of the basal ganglia based on similar images was demonstrated previously (Lenglet et al., 2012). Along with the T2-weighted images, these binary segmentations were rigidly coregistered to each subject's T1-space with FSL's FLIRT, using sinc interpolation with a Hanning window (Jenkinson et al., 2002). These segmentations were then binarized again using a threshold of 0.45, which was empirically determined to least affect the volumes of the segmentations.

2.3.3. Diffusion analysis—After correction for motion and for susceptibility and eddy current distortions with FSL's eddy and topup algorithms (Andersson et al., 2003), diffusion parameters were estimated using a three-fiber model with FSL's bedpostX (Behrens et al., 2007). Probabilistic fiber tracking with FSL's probtrackX2 was performed in T1-space, using a rigid transformation matrix, with the STN as a seed region and 500 samples per voxel (equivalent to 2315 samples per mm^3). Other fiber tracking settings included FSL's default curvature threshold of 0.2, maximum number of steps per sample of 2000, step length of 0.5 mm, subsidiary fiber volume threshold of 0.01, and termination of pathways that looped back on themselves. Using the ipsilateral cortex as inclusion region and the contralateral hemisphere as exclusion region, the percentage of tracks reaching either of the four ipsilateral cortical regions was computed for each voxel in the STN (Fig. 1). A voxel was considered to be connected to that cortical area if at least 25% of its probabilistic tracks connected the two, allowing for one voxel to be connected to more than one cortical area. This threshold was preferred over a winner-takes-all approach, because with a diffusion resolution of 1.5 mm isotropic, one voxel might contain several white matter tracks.

2.4. Validation

As a first step to validate our methods, we have used our protocol to map the known thalamic connections to the prefrontal-temporal, motor, somatosensory, and parieto-occipital cortical areas. The results were compared to the thalamic connectivity based segmentation as demonstrated by Behrens et al. (2003).

Secondly, in five STNs, the classification of the motor STN region was compared to the position of the active contact, by registering the post-surgery CT (showing the DBS lead) to our anatomical model. These contacts had been confirmed to stimulate the motor area of the STN, through intra-operative micro-electrode recording (MER), intra-operative testing, and post-operative surveys, and were confirmed by improved motor performance of the patients.

2.5. Reproducibility

In order to assess the reproducibility, a 26 years old healthy male subject was scanned four times on three different days with the same scan protocol as described in Section 2.2 and Table 1. The four datasets were then analyzed as described above and the reproducibility of the outcome results was assessed.

2.6. Statistical analysis

Volumes of the STN and of its subdivisions are presented as means and standard deviations. Statistical comparisons were made using the related samples Wilcoxon signed rank test to evaluate right and left differences in STN volumes. A p-Value < 0.05 was considered statistically significant.

3. Results

3.1. Validation

The first step of this study was to validate our analysis approach by reproducing the results of Behrens et al. (2003) (Fig. 2). This demonstrates that our methods allow us to create detailed parcellations of subcortical structures of individual PD patients.

3.2. STN segmentation

The mean volume of the segmented STNs in their native space across all patients was 125.4 mm^3 (± 22.9 mm^3). The biconvex structure was consistently oriented along an axis that ran from its superior posterolateral to its inferior anteromedial apex; the most anterior apex of the STN was also located at its most medial and most inferior border and its most posterior apex also formed its most lateral and most posterior ends. No significant differences were found between the volumes of the left and right STNs (p=0.52).

3.3. STN parcellation

A consistent functional organization was observed in all STNs, with the zones arranged mainly along its longest axis, as was visually assessed from 3D displays of the STNs. In all 34 STNs, the superior posterolateral division of the STN showed strong connections to the motor cortical areas, and a partly overlapping zone located centrally along the STN's longest axis was mainly connected to associative cortical areas. Connections to the limbic cortical brain areas could be identified in 30 of 34 STNs, originating from STN territories with varying volumes, but in all 30 cases located at the inferior anteromedial section of the STN. This ordering of the motor, associative, and limbic zones of the STN along the posterolateral-anteromedial axis is illustrated in three representative examples (Fig. 3). Connections of the STN to the remaining cortical regions were found as well, although they did not have a consistent origin within the STN and these zones were relatively small.

3.4. Volumes of the STN's functional zones

Fig. 4 illustrates the variations in the relative volumes of each zone, defined by a relative connectivity of at least 25%, between patients and hemispheres. The average volumes, per region, were 55.3% (± 14.0%) for the motor area, 55.6% (± 15.9%) for the associative area, 20.3% (± 16.3%) for the limbic area, and 12.5% (± 16.2%) for STN volumes connected to other cortical areas. This corresponds to volumes of 68.7 mm^3 (± 19.7 mm^3), 70.6 mm^3 (± 26.7 mm^3), 25.8 mm^3 (± 20.8 mm^3), and 16.1 mm^3 (± 21.0 mm^3) for the motor, associative, limbic and other cortical areas, respectively. Note that the percentages add up to more than 100%, because of overlap (as described in Section 2.3.), with 17.01% (± 8.85%) of the STN volume assigned to both motor and associative functions and 15.56% (± 13.15)

to both associative and limbic functions, corresponding to average volumes of 21.0 mm^3 and 19.3 mm^3 respectively.

3.5. Reproducibility

To examine the reliability of our findings, the same analysis was applied to four independently repeated scan sessions of a single healthy subject. Although there are some intra-subject variations of both the total STN volumes as well as the relative volumes of the subdivisions, they are consistently smaller than the inter-subject standard deviations among our patient population (Table 2 and Fig. 5). This example suggests adequate reproducibility of the methods and sensitivity to actual patient specific variations.

3.6. Overlap

The overlap of the subdivisions within the STN indicates that one voxel can be connected to more than one cortical mask. This is also reflected in the underlying probability maps of the connections of the STN to each cortical mask. Fig. 6 shows examples of these probability maps of three subject. This indicates that the functional zones indeed gradually transition into each other.

3.7. Illustrative cases of implanted electrodes in the motor part of the STN

Fig. 7 shows that the active contacts of five example cases, as defined during the post-surgery programming, indeed correspond to our predicted motor zones, which were created with solely non-invasive pre-operative data.

4. Discussion

Ultra-high field MR imaging has enabled us to reliably visualize the motor and non-motor zones of the STN of individual patients with PD referred for deep brain stimulation surgery. We expect that this will facilitate patient-specific and selective targeting of the motor part of the STN, thereby enhancing surgical planning at the level of the individual patient. Moreover, the possibility of more accurate image-guided placement has the potential to reduce surgery duration and/or perform surgery under general anesthesia, which both greatly reduce the burden on patients. In addition, the ability to fuse the postoperative CT images with the preoperative 7 T data allows for the visualization of the position of the electrode and contacts. This may provide vital information to determine the optimal location for implantation of DBS leads, not only within the STN, but also within the motor zone of the patient's STN. Additionally, the optimal lead location could potentially be used, in conjunction with volume tissue activated (VTA) models, to determine the best possible programming settings personalized to each patient.

Anatomical, behavioral, and electrophysiological studies have contributed to our understanding of the organization of the STN into subdivisions. Tracers injected in different territories of the primate external globus pallidus showed a segregated labeling of the STN (Karachi et al., 2005), and GABA agonist and antagonist injections into the posterior, medial, and anterior STN had different effects on behavioral and motor symptoms in non-human primates (Karachi et al., 2009). Similarly, electrophysiological recordings in patients

with PD localized the neurons activated in limb movement (motor region) in the dorsolateral region of the STN (Rodriguez-Oroz et al., 2001). This parcellation has also been investigated in MRI studies of healthy subjects at 3 T. One study investigating the STN's connectivity in twelve healthy subjects showed that there are most probably three connectivity clusters within the STN related to motor, associative, and limbic functions (Lambert et al., 2012). The averaged locations of these zones in healthy subjects correspond with our findings in individual patients. This arrangement was also observed in another 3 T functional and structural connectivity study based on averaged data of healthy subjects, but could not be demonstrated consistently in all individual subjects (Brunenberg et al., 2012). Finally the STN's connectivity was previously investigated in PD patients as well, although this only concerned its motor area and analyses were only performed in a qualitative manner (Avecillas-Chasin et al., 2015). Here, we show that the three zones can also be objectively and quantitatively identified in patients with PD and, importantly, on an individual basis. With these methods there is no need to average the data to create a general STN model, but rather, patient-specific and individual models for each patient can be created.

We have found a considerable overlap between the different segmented zones of the STN. Two possible explanations could account for these results; first, the probabilistic nature of the applied connectivity measure and partial volume effects allow for multiple connections per individual voxel. Second, the overlap may indeed reflect the actual pathways that are not segregated but partially integrated. This is in line with a tracing study in non-human primates showing overlapping projections from M1 to the dorsolateral STN and from prefrontal cortical areas to the anterior, ventral, and medial half of the STN (Haynes and Haber, 2013). It is known that STN neurons located in the border zones receive multiple inputs and are responsible for the integration of information from different cortical regions performing different functions. To what extend stimulation of this overlapping area will result in beneficial motor effects or unwanted side-effects, remains to be seen.

The average STN volume that we found (125.4 mm^3) is in line with previous findings (Lambert et al., 2012; Massey et al., 2012). A variation in the total volumes exists and is reflected also in the relative volumes of the different functional zones. However, regardless of this variability, we also found a few outliers of exceptionally small associative (n=1), motor (n=2), or limbic zones (n=9). In addition, in some cases we observed deviations of the arrangement of the functional zones, in the sense that the one STN territory showed small protrusions into another territory to a larger extend than the expected overlap. Finally, we observed sporadic connections to the remaining cortical areas. These deviations might be the result of false positives and negatives inherent to probabilistic tractography. Nevertheless, the relatively small contribution of the remaining cortical area to the STNs' maps indicates that the reconstructed connectivity we found here represents actual anatomical connections. Despite these few deviations, in all 34 STNs, the posterolateral portion was consistently connected to the motor cortical areas.

Our data and methods were validated by reproducing the earlier demonstrated connectivity based parcellation of the thalamus (Behrens et al., 2003). Our results are very similar to the established segregation of the thalamus, demonstrating that our ultra-high field MRI data and methods are suitable for parcellating subcortical structures, with considerably shorter

scan times. The small discrepancies found between our and Behrens's et al. thalamic parcellation may be explained by underlying differences between subjects, discrepancies in the definitions of the cortical areas, or differences in the orientation and location of the visualized cut through the thalamus. Furthermore, the STN parcellation was validated with the final DBS electrode location in five example cases. We confirm that the active contacts, as determined by the MER during surgery and the programming post-surgery, were indeed located within the motor zone as defined by this work. This illustrates its future potential value.

To assess the reproducibility of our methods, the measurements and analyses were repeated four times on one subject. Although the numbers are too small to reliably assess significance, the within subject standard deviation was smaller than the between subject standard deviation for both the total STN volumes and all volumes of the sub-territories. This suggests that the variability that we find between patients can, at least partially, be explained by the underlying variability in the patients' anatomy; thus providing a detailed mapping of the patient's own STN, not based on a standard and common anatomical atlas, which should have a high priority for enhancing targeting accuracy for DBS surgeries. Furthermore, the fact that similar results were produced with datasets collected at two different centers (with small differences in the scanning protocols), also indicates that the used analysis pipeline is robust and independent of acquisition parameters.

The clear visualization of the STN and relatively short scan times, combined with the high-resolution parcellation of the STN, result from the known benefits of ultra-high field MRI (Duyn, 2012; Vaughan et al., 2001; Yacoub et al., 2008) and demonstrate its clinical utility. Although 7T MR scanners are not yet accessible for all DBS centers, their numbers are growing quickly; in fact, an FDA approved system is expected to be released in the near future.

There are a few limiting factors that are inherent to high-resolution MRI and structural connectivity mapping of brain structures. For one, movement artifacts are an obvious limitation when scanning movement disorder patients. They were minimized by using scan protocols that were optimized for this patient group (Abosch et al., 2010; Lenglet et al., 2012). Second, ultra-high field diffusion imaging is sensitive to signal loss in the temporal lobes (Polders et al., 2011). To partly overcome these problems, dielectric pads were used if they could be fitted comfortably. Nevertheless, this issue may explain why the observed connections to the limbic regions in the temporal and orbitofrontal areas were less prominent than expected. Also, contrary to, for example, tracing or electrophysiological studies, diffusion-based tractography cannot infer information on the signaling direction of the connections. In addition connections occurring at a much smaller scale than the imaging resolution, such as disynaptic connections, have been ignored in the analyses. Furthermore, sampling the distribution of diffusion directions in each step, using probabilistic tractography will result in some false positives and false negatives depending on data quality, track length, crossing fiber areas, and partial volume effects. The latter of those, which may have occurred in voxels bordering the STN, might further explain the tracked connections to the remaining cortical areas. It may also account for the variability in observed volume of the limbic zone of the STN, which was previously demonstrated to extend to the neighboring

lateral hypothalamus in primates (Haynes and Haber, 2013). In addition, the threshold method that was used to visualize the functional zones within the STN shows them as hard boundaries. However, this is inherent to the applied threshold as is reflected by the additionally demonstrated gradual overlap between the zones. Furthermore, we only considered the cortico-subthalamic connections. Although the subcortical connections of the STN underpin its important role in the basal ganglia (Lenglet et al., 2012; Parent and Hazrati, 1995), creating functional segregation maps from them is difficult because of the complex interplay of different functions. The functional segregation of the cortex and especially of the motor cortical areas is much better understood and their large surface areas make them more robust to small segmentation errors in the cortex. Therefore, using the cortical segmentations to functionally subdivide the STN is likely more realistic than using the basal ganglia connections. Finally, the number of zones detected within the STN is related to the predefined number of cortical segmentations and can in this study not exceed four. Using a clustering algorithm to parcellate the cortex and STN, might result in a more individualized number of clusters. Future studies, with submillimeter spatial resolution, will address the clustering approach to determine the number of zones independently.

Although the ability to identify the different sub-territories of the STN is a leap forward in the process of direct targeting, more extensive study is needed to bring it to clinical practice. Furthermore, the methods developed here, open new doors for a better understanding of Parkinson's disease and its treatments. Comparisons with healthy control subjects may provide new insight into the pathologic anatomy in PD. Moreover, the proposed methods may lead to a better understanding of what circuits are being stimulated and how this affects patient outcome.

5. Conclusion

The motor part of the STN is the main target in deep brain stimulation surgery for patients with PD. Using ultra-high field MR technology and tractography-based data analysis methods, we have provided a proof of concept for identifying the motor and non-motor zones of the STN in individual patients. We have observed that there is a substantial variation between individuals with PD. This type of new data may potentially allow for optimized surgical planning at the level of the individual patient preoperatively and create the possibility of patient-specific targeting and programming of the DBS therapy post-operatively. We see this as a critical step towards development of patient specific deep brain stimulation for PD.

Acknowledgments

This study was supported by grants of the Netherlands Organisation for Scientific Research (NWO, Grant no. 452-11-002), the Netherlands Organisation for Health Research and Development (ZonMW, Grant no. ZonMW/116350003/JSTP), the National Institutes of Health (NIH, Grant nos. R01-NS085188, P41-EB015894 and P30-NS076408), and the University of Minnesota Udall center (P50NS098573). The authors would like to thank Dimo Ivanov for his help with the scans.

Abbreviations

DBS deep brain stimulation

PD	Parkinson’s disease
STN	subthalamic nucleus

References

Abosch A, Yacoub E, Ugurbil K, Harel N. An assessment of current brain targets for deep brain stimulation surgery with susceptibility-weighted imaging at 7 T. Neurosurgery. 2010; 67:1745–1756. [PubMed: 21107206]

Alkemade A, Forstmann BU. Do we need to revise the tripartite subdivision hypothesis of the human subthalamic nucleus (STN)? Neuroimage. 2014; 95:326–329. [PubMed: 24642281]

Andersson JL, Skare S, Ashburner J. How to correct susceptibility distortions in spin-echo echo-planar images: application to diffusion tensor imaging. Neuroimage. 2003; 20:870–888. [PubMed: 14568458]

Andersson, JLR., Jenkinson, M., Smith, S. Non-Linear Registration Aka Spatial Normalisation FMRIB Centre. Oxford; United Kingdom: 2007.

Avecillas-Chasin JM, Alonso-Frech F, Parras O, Del Prado N, Barcia JA. Assessment of a method to determine deep brain stimulation targets using deterministic tractography in a navigation system. Neurosurg Rev. 2015; 38:739–751. [PubMed: 25962557]

Behrens TE, Berg HJ, Jbabdi S, Rushworth MF, Woolrich MW. Probabilistic diffusion tractography with multiple fibre orientations: what can we gain? Neuroimage. 2007; 34:144–155. [PubMed: 17070705]

Behrens TE, Johansen-Berg H, Woolrich MW, Smith SM, Wheeler-Kingshott CA, Boulby PA, Barker GJ, Sillery EL, Sheehan K, Ciccarelli O, Thompson AJ, Brady JM, Matthews PM. Non-invasive mapping of connections between human thalamus and cortex using diffusion imaging. Nat Neurosci. 2003; 6:750–757. [PubMed: 12808459]

Brunenberg EJL, Moeskops P, Backes WH, Pollo C, Cammoun L, Vilanova A, Janssen MLF, Visser-Vandewalle VERM, Ter Haar Romeny BM, Thiran JP, Platel B. Structural and resting state functional connectivity of the subthalamic nucleus: identification of motor STN parts and the hyperdirect pathway. PLoS One. 2012; 7:e39061. [PubMed: 22768059]

Cho ZH, Min HK, Oh SH, Han JY, Park CW, Chi JG, Kim YB, Paek SH, Lozano AM, Lee KH. Direct visualization of deep brain stimulation targets in Parkinson disease with the use of 7-T magnetic resonance imaging. J Neurosurg. 2010; 113:639–647. [PubMed: 20380532]

Desikan RS, Segonne F, Fischl B, Quinn BT, Dickerson BC, Blacker D, Buckner RL, Dale AM, Maguire RP, Hyman BT, Albert MS, Killiany RJ. An automated labeling system for subdividing the human cerebral cortex on MRI scans into gyral based regions of interest. Neuroimage. 2006; 31:968–980. [PubMed: 16530430]

Deuschl G, Schade-Brittinger C, Krack P, Volkmann J, Schafer H, Botzel K, Daniels C, Deutschlander A, Dillmann U, Eisner W, Gruber D, Hamel W, Herzog J, Hilker R, Klebe S, Kloss M, Koy J, Krause M, Kupsch A, Lorenz D, Lorenzl S, Mehdorn HM, Moringlane JR, Oertel W, Pinsker MO, Reichmann H, Reuss A, Schneider GH, Schnitzler A, Steude U, Sturm V, Timmermann L, Tronnier V, Trottenberg T, Wojtecki L, Wolf E, Poewe W, Voges J. A randomized trial of deep-brain stimulation for Parkinson’s disease. New Engl J Med. 2006; 355:896–908. [PubMed: 16943402]

Duyn JH. The future of ultra-high field MRI and fMRI for study of the human brain. Neuroimage. 2012; 62:1241–1248. [PubMed: 22063093]

Grabner, G., Janke, A., Budge, M., Smith, D., Pruessner, J., Collins, DL. Symmetric atlasing and model based segmentation: an application to the hippocampus in older adults. In: Larsen, R.Nielsen, M., Sporring, J., editors. Medical Image Computing and Computer-Assisted Intervention – MICCAI. Springer; Berlin, Heidelberg: 2006. p. 58-66.2006

Haynes WI, Haber SN. The organization of prefrontal-subthalamic inputs in primates provides an anatomical substrate for both functional specificity and integration: implications for basal ganglia models and deep brain stimulation. J Neurosci. 2013; 33:4804–4814. [PubMed: 23486951]

Jenkinson M, Bannister P, Brady M, Smith S. Improved optimization for the robust and accurate linear registration and motion correction of brain images. Neuroimage. 2002; 17:825–841. [PubMed: 12377157]

Karachi C, Grabli D, Baup N, Mounayar S, Tande D, Francois C, Hirsch EC. Dysfunction of the subthalamic nucleus induces behavioral and movement disorders in monkeys. Mov Disord. 2009; 24:1183–1192. [PubMed: 19412950]

Karachi C, Yelnik J, Tande D, Tremblay L, Hirsch EC, Francois C. The pallidosubthalamic projection: an anatomical substrate for nonmotor functions of the subthalamic nucleus in primates. Mov Disord. 2005; 20:172–180. [PubMed: 15382210]

Keuken MC, Uylings HB, Geyer S, Schafer A, Turner R, Forstmann BU. Are there three subdivisions in the primate subthalamic nucleus? Front Neuroanat. 2012; 6:14. [PubMed: 22590455]

Lambert C, Zrinzo L, Nagy Z, Lutti A, Hariz M, Foltynie T, Draganski B, Ashburner J, Frackowiak R. Confirmation of functional zones within the human subthalamic nucleus: patterns of connectivity and sub-parcellation using diffusion weighted imaging. Neuroimage. 2012; 60:83–94. [PubMed: 22173294]

Lambert C, Zrinzo L, Nagy Z, Lutti A, Hariz M, Foltynie T, Draganski B, Ashburner J, Frackowiak R. Do we need to revise the tripartite subdivision hypothesis of the human subthalamic nucleus (STN)? Response to Alkemade and Forstmann. Neuroimage. 2015; 110:1–2. [PubMed: 25620491]

Lenglet C, Abosch A, Yacoub E, De Martino F, Sapiro G, Harel N. Comprehensive in vivo mapping of the human basal ganglia and thalamic connectome in individuals using 7T MRI. PLoS One. 2012; 7:e29153. [PubMed: 22235267]

Mai, JK., Paxinos, G., Voss, T. Atlas of the HumanBrain. Academic Press; 2008.

Mallet L, Schupbach M, N'Diaye K, Remy P, Bardinet E, Czernecki V, Welter ML, Pelissolo A, Ruberg M, Agid Y, Yelnik J. Stimulation of subterritories of the subthalamic nucleus reveals its role in the integration of the emotional and motor aspects of behavior. Proc Natl Acad Sci USA. 2007; 104:10661–10666. [PubMed: 17556546]

Massey LA, Miranda MA, Zrinzo L, Al-Helli O, Parkes HG, Thornton JS, So PW, White MJ, Mancini L, Strand C, Holton JL, Hariz MI, Lees AJ, Revesz T, Yousry TA. High resolution MR anatomy of the subthalamic nucleus: imaging at 9.4 T with histological validation. Neuroimage. 2012; 59:2035–2044. [PubMed: 22036997]

Mayka MA, Corcos DM, Leurgans SE, Vaillancourt DE. Three-dimensional locations and boundaries of motor and premotor cortices as defined by functional brain imaging: a meta-analysis. Neuroimage. 2006; 31:1453–1474. [PubMed: 16571375]

Okun MS, Fernandez HH, Wu SS, Kirsch-Darrow L, Bowers D, Bova F, Suelter M, Jacobson CEt, Wang X, Gordon CW Jr, Zeilman P, Romrell J, Martin P, Ward H, Rodriguez RL, Foote KD. Cognition and mood in Parkinson's disease in subthalamic nucleus versus globus pallidus interna deep brain stimulation: the COMPARE trial. Ann Neurol. 2009; 65:586–595. [PubMed: 19288469]

Okun MS, Tagliati M, Pourfar M, Fernandez HH, Rodriguez RL, Alterman RL, Foote KD. Management of referred deep brain stimulation failures: a retrospective analysis from 2 movement disorders centers. Arch Neurol. 2005; 62:1250–1255. [PubMed: 15956104]

Paek SH, Yun JY, Song SW, Kim IK, Hwang JH, Kim JW, Kim HJ, Kim HJ, Kim YE, Lim YH, Kim MR, Huh JH, Lee KM, Park SK, Kim C, Kim DG, Jeon BS. The clinical impact of precise electrode positioning in STN DBS on three-year outcomes. J Neurol Sci. 2013; 327:25–31. [PubMed: 23465484]

Parent A, Hazrati LN. Functional anatomy of the basal ganglia. II. The place of subthalamic nucleus and external pallidum in basal ganglia circuitry. Brain Res Rev. 1995; 20:128–154. [PubMed: 7711765]

Plantinga BR, Temel Y, Roebroeck A, Uludag K, Ivanov D, Kuijf ML, Ter Haar Romenij BM. Ultra-high field magnetic resonance imaging of the basal ganglia and related structures. Front Hum Neurosci. 2014; 8:876. [PubMed: 25414656]

Polders DL, Leemans A, Hendrikse J, Donahue MJ, Luijten PR, Hoogduin JM. Signal to noise ratio and uncertainty in diffusion tensor imaging at 1.5, 3.0, and 7.0 T. J Magn Reson Imaging. 2011; 33:1456–1463. [PubMed: 21591016]

Rodriguez-Oroz MC, Rodriguez M, Guridi J, Mewes K, Chockkman V, Vitek J, DeLong MR, Obeso JA. The subthalamic nucleus in Parkinson's disease: somatotopic organization and physiological characteristics. Brain. 2001; 124:1777–1790. [PubMed: 11522580]

Schuepbach WM, Rau J, Knudsen K, Volkmann J, Krack P, Timmermann L, Halbig TD, Hesekamp H, Navarro SM, Meier N, Falk D, Mehdorn M, Paschen S, Maarouf M, Barbe MT, Fink GR, Kupsch A, Gruber D, Schneider GH, Seigneuret E, Kistner A, Chaynes P, Ory-Magne F, Brefel Courbon C, Vesper J, Schnitzler A, Wojtecki L, Houeto JL, Bataille B, Maltete D, Damier P, Raoul S, Sixel-Doering F, Hellwig D, Gharabaghi A, Kruger R, Pinsker MO, Amtage F, Regis JM, Witjas T, Thobois S, Mertens P, Kloss M, Hartmann A, Oertel WH, Post B, Speelman H, Agid Y, Schade-Brittinger C, Deuschl G. Neurostimulation for Parkinson's disease with early motor complications. New Engl J Med. 2013; 368:610–622. [PubMed: 23406026]

Teeuwisse WM, Brink WM, Webb AG. Quantitative assessment of the effects of high-permittivity pads in 7 Tesla MRI of the brain. Magn Reson Med: Offi J Soc Magn Reson Med/Soc Magn Reson Med. 2012; 67:1285–1293.

Temel Y, Blokland A, Steinbusch HWM, Visser-Vandewalle V. The functional role of the subthalamic nucleus in cognitive and limbic circuits. Prog Neurobiol. 2005; 76:393–413. [PubMed: 16249050]

Vaughan JT, Garwood M, Collins CM, Liu W, DelaBarre L, Adriany G, Andersen P, Merkle H, Goebel R, Smith MB, Ugurbil K. 7T vs. 4T: RF power, homogeneity, and signal-to-noise comparison in head images. Magn Reson Med: Offi J Soc Magn Reson Med/Soc Magn Reson Med. 2001; 46:24–30.

Welter ML, Schupbach M, Czernecki V, Karachi C, Fernandez-Vidal S, Golmard JL, Serra G, Navarro S, Welaratne A, Hartmann A, Mesnage V, Pineau F, Cornu P, Pidoux B, Worbe Y, Zikos P, Grabli D, Galanaud D, Bonnet AM, Belaid H, Dormont D, Vidailhet M, Mallet L, Houeto JL, Bardinet E, Yelnik J, Agid Y. Optimal target localization for subthalamic stimulation in patients with Parkinson disease. Neurology. 2014; 82:1352–1361. [PubMed: 24647024]

Yacoub E, Harel N, Ugurbil K. High-field fMRI unveils orientation columns in humans. Proc Natl Acad Sci USA. 2008; 105:10607–10612. [PubMed: 18641121]

Zaidel A, Spivak A, Grieb B, Bergman H, Israel Z. Subthalamic span of beta oscillations predicts deep brain stimulation efficacy for patients with Parkinson's disease. Brain. 2010; 133:2007–2021. [PubMed: 20534648]

Zhang Y, Brady M, Smith S. Segmentation of brain MR images through a hidden Markov random field model and the expectation-maximization algorithm. IEEE Trans Med Imaging. 2001; 20:45–57. [PubMed: 11293691]

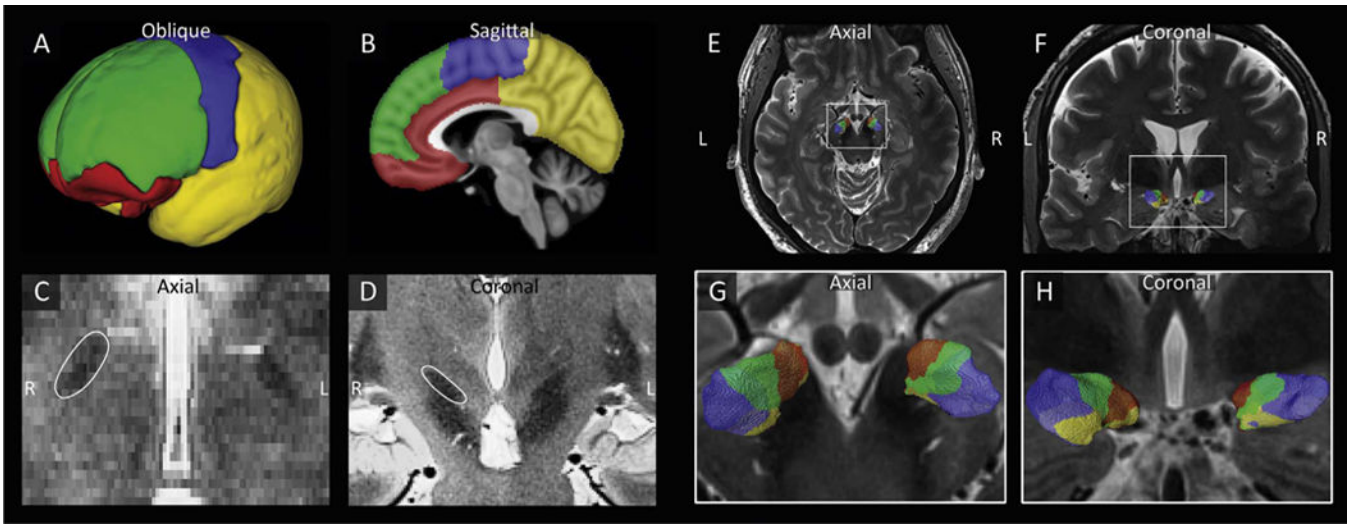

Fig. 1.

The STN is parcellated based on its connections to the limbic, associative, motor, and remaining cortical areas. A–B) Division of the cortex into limbic (red), associative (green), motor (blue) and remaining (yellow) cortical areas. C–D) Visualization of the hypointense STNs in the axial (C) and coronal (D) planes. E–H) Example of the parcellation of the STNs of one subject in axial (E,G) and coronal (F,H) views.

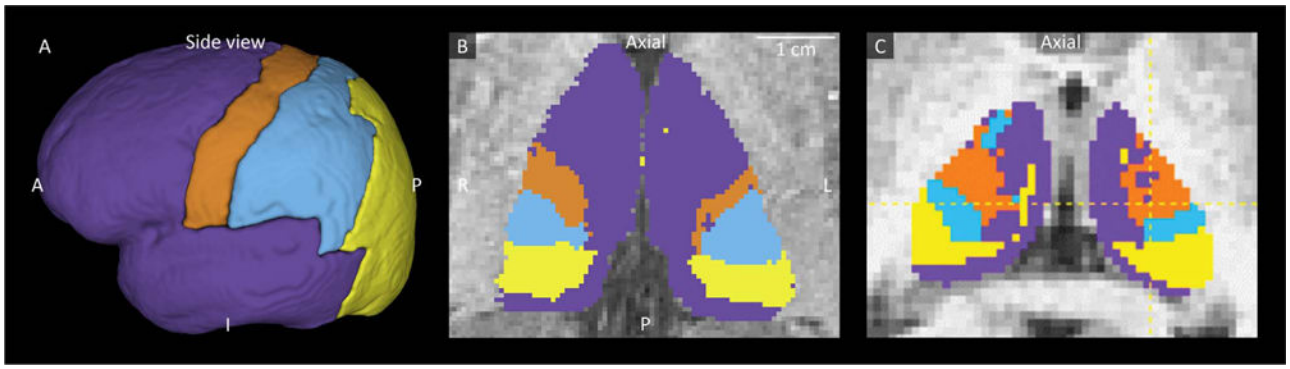

Fig. 2.

Connectivity mapping of the thalamus. A) Manual segmentation of the cortex into prefrontal and temporal (purple), motor (orange), somatosensory (blue), and parieto-occipital (yellow) cortical areas as defined by Behrens et al. (2003). B) A patient specific thalamic subdivision in one of our subjects. C) Thalamic subdivision as demonstrated by Adopted from Behrens et al. (2003).

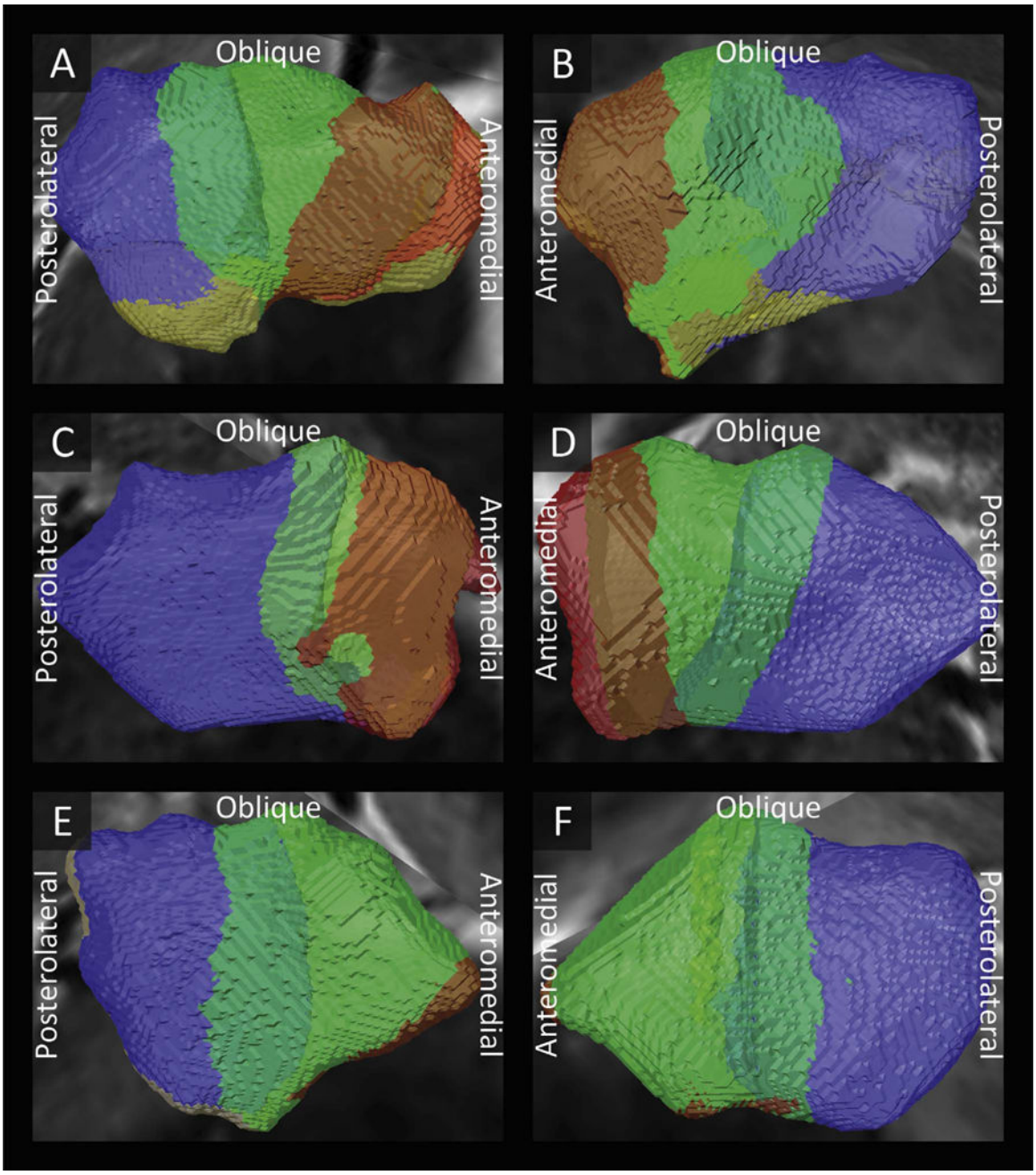

Fig. 3.

Examples of the subdivisions of the left (A,C,E) and right (B,D,F) subthalamic nuclei of three subjects into a limbic (red), associative (green), and motor (blue) zone. Intermediate colors show overlap between the motor and associative zones (light blue) and between the associative and limbic zones (brown).

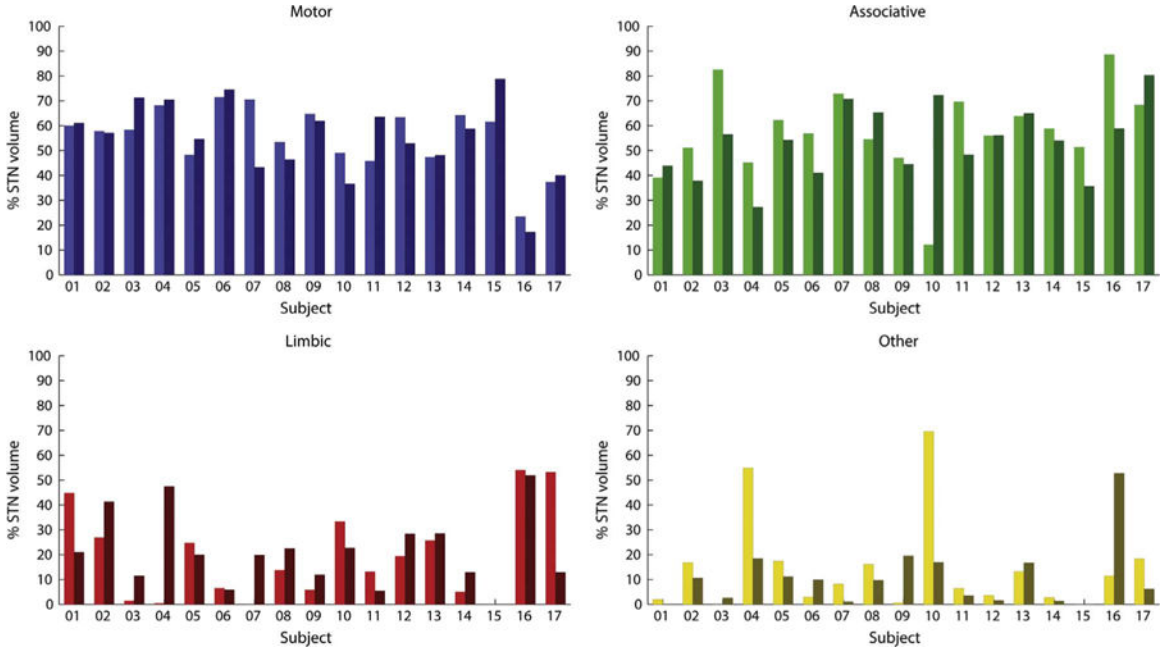

Fig. 4.

Relative volumes of each functional zone compared to the total STN volume within the left and right STN (left and right bar) of each subject.

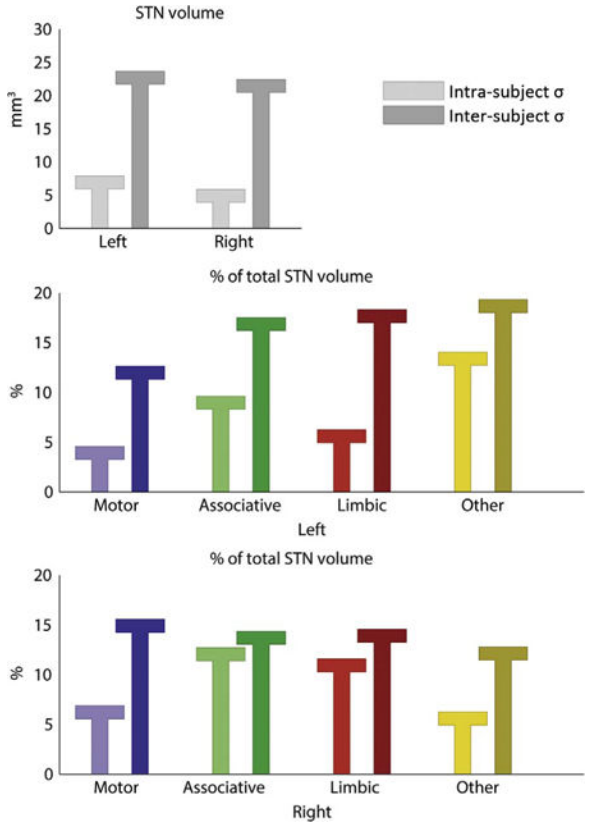

Fig. 5.

Comparison of the intra-subject (light bars) standard deviations (σ) and inter-subject (dark bars) standard deviations of the volumes of the subthalamic nucleus (STN) and the relative volumes of the zones.

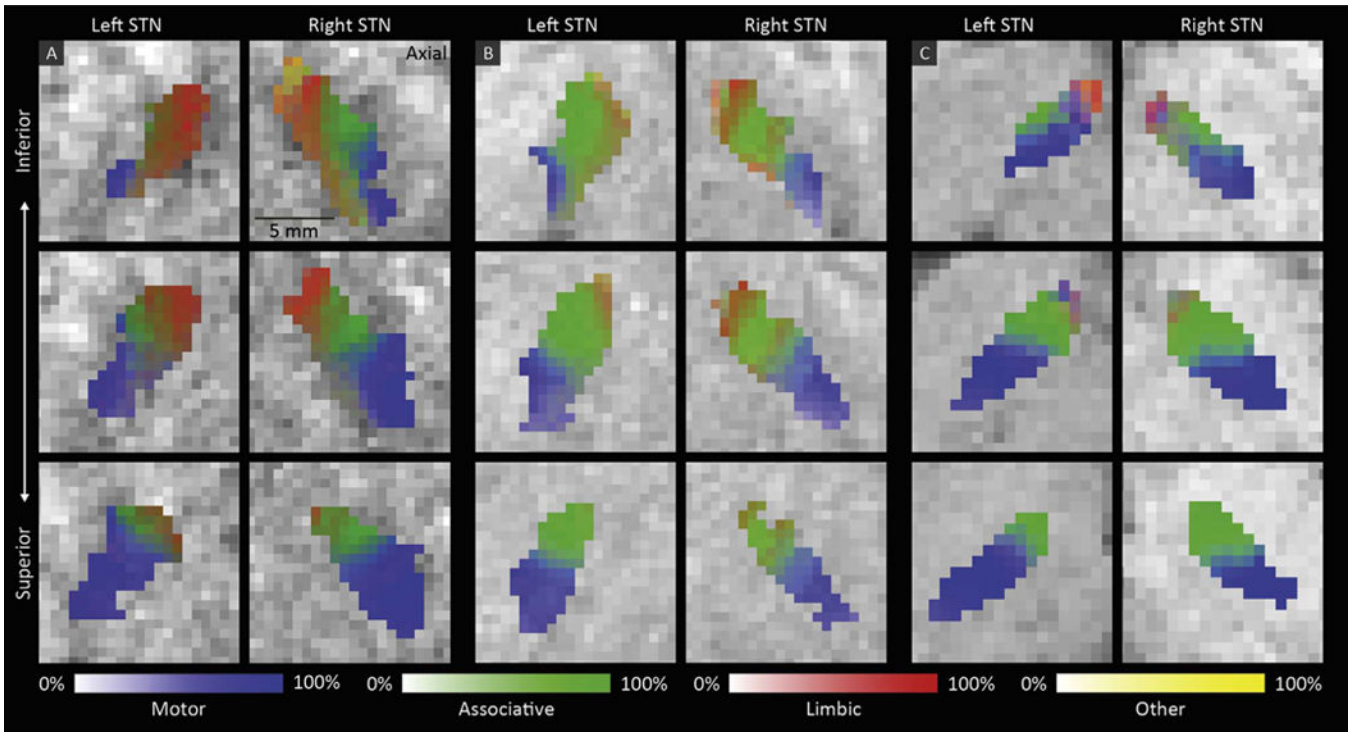

Fig. 6.

The percentage of connectivity to the motor (blue), associative (green), limbic (red) and remaining (yellow) cortical areas in three axial slices through the left and right STN ordered from inferior to superior in three subjects (A, B, and C).

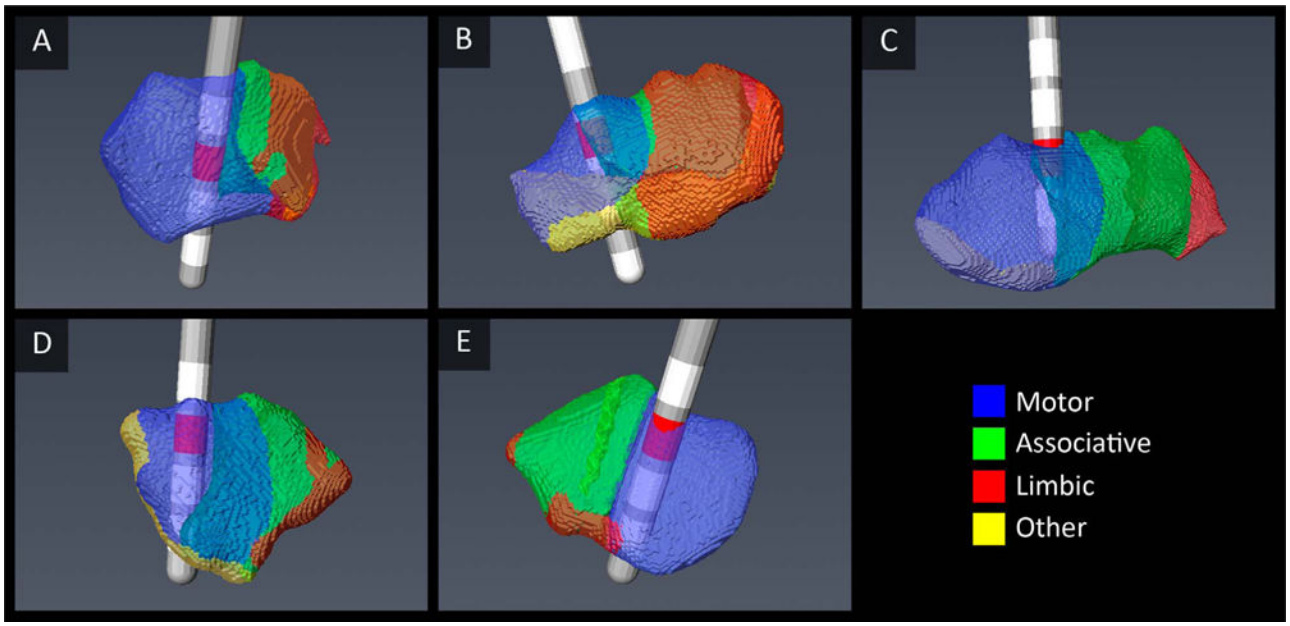

Fig. 7.
Examples of the electrode position in five STNs. The active contacts (red) lie within the computed motor areas.

Table 1

Scan sequence parameters.

Weighting	Sequence	TE (ms)	TR (ms)	Flip angle (°)	Matrix size (x×y×z)	Resolution (mm^3) (x×y×z)	Acquisition time (min)
T1	3D GR/IR	3.5	3100	5	312×384×256	0.6×0.6×0.6	6.5
T2	2D SE	58	± 8000	150	512×26×512	0.39×1.0×0.39	6.5
Diffusion	2D EP	55.6	± 5000	90	136×136×66	1.5×1.5×1.5	2×4.5

GR/IR=gradient-recalled echo/inversion recovery. TE=echo time. TR=repetition time. SE=spin echo. EP=echo planar.

Table 2

Standard deviations of the STN volumes (mm^3) and the relative volumes of their functional zones (%).

Area	Left					Right				
	STN	**Motor**	**Associative**	**Limbic**	**Other**	**STN**	**Motor**	**Associative**	**Limbic**	**Other**
Within subject	7.9	4.58	9.63	6.25	14.03	5.87	6.86	12.7	11.58	6.24
Between subject	23.69	12.61	17.52	18.32	19.32	22.43	15.57	14.36	14.57	12.78